DOI: 10.1002/chem.201003080

Cobalt Imidazolate Framework as Precursor for Oxygen Reduction Reaction Electrocatalysts

Shengqian Ma,[a] Gabriel A. Goenaga,[a] Ann V. Call,[b] and Di-Jia Liu*[a]

We demonstrate a new approach of preparing a non-platinum group metal (PGM) electrocatalyst for oxygen reduction reaction through rational design by using cobalt imidazolate framework—a subclass of metal-organic framework (MOF) material—as the precursor with potential to produce uniformly distributed catalytic center and high active-site density.

MOFs[1] represent a new type of materials, and have recently been under broad exploration of various important applications[2] due to their amenability to rational design for different functionalities at molecular level.[3] In particular, their high surface areas, well-defined porous structures, and building block variety[4] not only distinguish them from the conventional materials in gas adsorption and separation,[5] but also offer new promises in catalysis application.[6] However, the application of porous MOFs for electrocatalysis in fuel cell has yet to be exploited.

The oxygen reduction reaction (ORR) at the cathode of a proton exchange membrane fuel cell (PEMFC) represents a very important electrocatalytic reaction. At present, the catalyst materials of choice are platinum group metals (PGMs).[7] The high costs and limited reserves of PGMs, however, created a major barrier for large-scale commercialization of PEMFCs.[8] Intensive efforts have been dedicated to the search of low-cost alternatives.[7] The discovery of ORR activity on cobalt phthalocyanine[9] stimulated extensive investigations of using Co–N_4 or Fe–N_4 macromolecules as precursors for preparation of transition metal (TM) based, non-PGM catalysts.[10] The ORR activity over a cobalt–polypyrrole composite was observed, of which a Co ligated by pyrrolic nitrogens was proposed as the catalytic site.[11] Activation in an inert atmosphere of the similar TM–polymer composite through pyrolysis further improved the catalytic activity.[12] More recently, significant enhancement in ORR activity was demonstrated in a carbon-supported iron-based catalysts, and it was suggested that micropores (width <20 Å) have critical influence on the formation of the active site with an ionic Fe coordinated by four pyridinic nitrogens after high-temperature treatment.[13] The onset potential for an Fe-based catalyst is found to be 0.1 V higher than that of a Co-based system although the latter is more stable under PEMFC operating condition.[7] These previous studies proposed the nitrogen-ligated TM entities either as the precursors or the active centers for the catalytic ORR process. Another challenge for non-PGM ORR catalysts is their relatively low turn-over-frequency in comparison with Pt.[14] To compensate low activity without using excessive amount of catalyst, thus causing thick electrode layer and poor mass transport, it is desirable to produce the highest possible catalytic-site density, that are evenly distributed and accessible to gas diffusion through a porous framework.

Herein we report the first experimental demonstration of porous MOF as a new class of precursor for preparing ORR catalysts. Different from previous approaches, MOFs have the following advantages when used to prepare non-PGM electrocatalysts: MOFs have clearly-defined three-dimensional structures. The initial entities such as TM–N_4 can be grafted into MOFs with the highest possible volumetric density through regularly arranged cell structure.[2b] The MOF surface area and pore size are tunable by the length of the linker. The organic linkers would be converted to carbon during thermal activation while maintaining the porous framework, leading to catalysts with high surface area and uniformly distributed active sites without the need of a second carbon support or pore forming agent. Furthermore, the TM–ligand composition can be rationally designed with wide selection of metal–linker combinations for systematical investigation on the relationship between precursor structure and catalyst activity. Our studies demonstrate the initial step to achieve such advantages.

[a] Dr. S. Ma, Dr. G. A. Goenaga, Dr. D.-J. Liu
Chemical Sciences & Engineering Division
Argonne National Laboratory, Argonne, IL 60439 (USA)
Fax: (+1) 630-252-4176
E-mail: djliu@anl.gov

[b] A. V. Call
Department of Materials Science and Engineering
Northwestern University, Evanston, IL 60208 (USA)

Supporting information for this article is available on the WWW under http://dx.doi.org/10.1002/chem.201003080.

We selected the cobalt imidazolate frameworks as the initial candidates for this study, because each cobalt atom is coordinated with four nitrogen atoms of imidazolate ligands (Figure 1 a) and the Co–N_4 moieties are all regularly distrib-

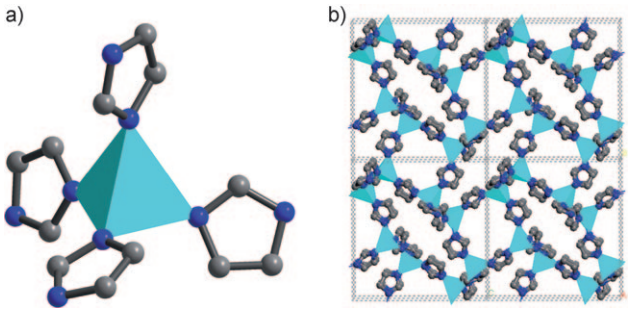

Figure 1. a) Local Co–N_4 coordination moiety; b) structure packing of **1** along the [100] direction (color scheme: turquoise = Co, blue = N, gray = C).

uted within the frameworks. Under solvothermal conditions, the reaction between the 3,5-imidazolate and $Co(NO_3)_2{\cdot}6H_2O$ in *N*,*N*′-dimethylacetamide (DMA) afforded purple crystals of the cobalt imidazolate framework **1**. Single-crystal X-ray studies revealed that **1** crystallizes in the space group $P2_1/n$, and has the same structure as a previously reported cobalt imidazolate compound.[15] In **1**, every cobalt atom binds four nitrogen atoms from four 3,5-imidazolate ligands and each 3,5-imidazolate ligand connects with two cobalt atoms to form a three-dimensional porous structure with Co–Co distance of approximately 8.1 Å along the [100] direction (Figure 1 b). The number of Co–N_4 moieties in the single crystal of **1** can reach as high as 3.6×10^{21} cm^{-3} (based on the crystal density of 1.162 $g\,cm^{-3}$). The N_2 adsorption isotherm measurement at 77 K shows that solvent-free **1** possesses permanent porosity with a Brunauer–Emmett–Teller (BET) specific surface area (SSA) of 305 $m^2\,g^{-1}$ (Figure S1 in the Supporting Information).

The crystalline compound **1** was subsequently heat-treated to produce an ORR catalyst. Co-based ORR catalysts are known to be more tolerant to the acidic environment in the PEMFC cathode even though the onset potential is typically around 0.1 volt less than that of Fe-based materials.[7] Rotating ring disk electrode (RRDE) measurement on the fresh **1** sample revealed little ORR activity, presumably due to the insulating nature of the organic framework. The activity, however, was substantially enhanced after the sample was heat-activated at different temperatures under an Ar atmosphere, as is shown in Figure 2. The sample started to demonstrate ORR activity after heated at 600 °C with an onset potential of 0.77 V. An optimal performance was achieved for the sample pyrolyzed at a temperature of 750 °C with an onset potential of 0.83 V, which is comparable to the best cobalt-based non-PGM catalysts.[7] The *I*–*V* curve also shows a rapid increase of the current density as the function of polarization voltage with half-wave potential of 0.68 V ob-

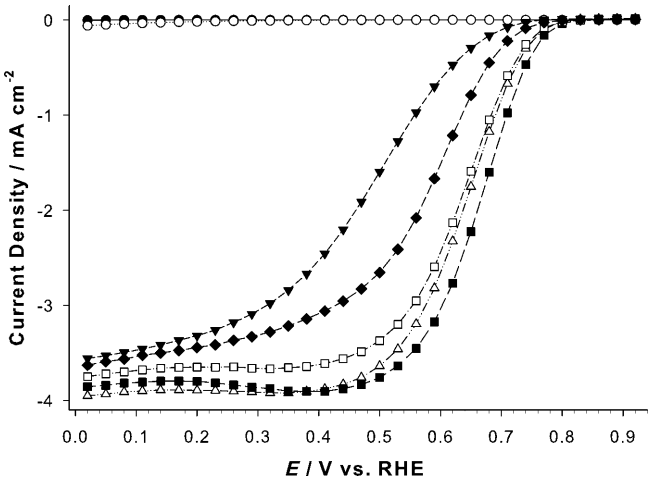

Figure 2. Faradaic current density as a function of the potential with reference to the reversible hydrogen electrode (RHE) for **1** at different temperatures (● = fresh sample, T = 500 (○), 600 (▼), 700 (△), 750 (■), 800 (□), and 900 °C (◆); rotating speed = 1600 rpm, catalyst loading = 600 $\mu g\,cm^{-2}$). The measurements were taken in 0.1 M $HClO_4$ solution saturated by oxygen at 25 °C.

served. Further increase of pyrolyzing temperature deteriorates the ORR activity.

Figure 3 shows the Tafel plot of the mass activity I_m, at different potential for **1** activated at 750 °C. Also shown in Figure 3 is the Tafel plot for the same sample after being

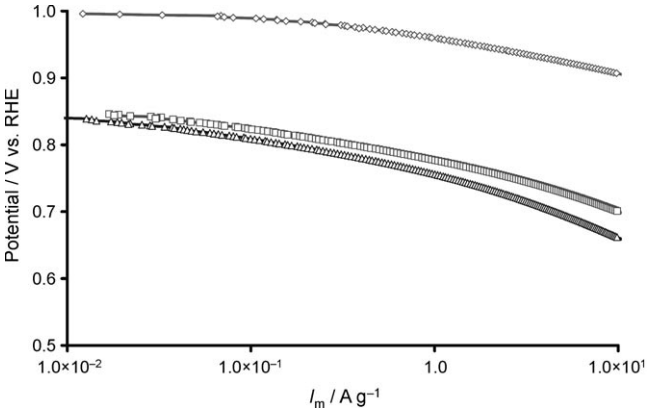

Figure 3. Tafel plots of the potential versus the mass activity for **1** activated at 750 °C (△), **1** activated at 750 °C and then washed with sulfuric acid (□), and Pt in 20 wt% Pt/C (◇). Experimental conditions are the same as given in Figure 2.

treated by sonicating in sulfuric acid to remove metallic cobalt formed during thermal treatment. For comparison, a similar Tafel plot for 20 wt % Pt/C (BASF) measured under the same test condition is also shown. The mass activity I_m is derived from Equation (1):

$$I_m = -I_k/m_{cat} \quad (1)$$

where I_k is the kinetic current and m_{cat} represents the mass

of the catalyst.[16] For activated **1**, m_{cat} equals the total amount of catalyst used whereas for the Pt/C catalyst m_{cat} is calculated based on the platinum loading only. For activated **1**, the mass activity reaches 0.05 $A g^{-1}$ at 0.8 V or 0.6 $A g^{-1}$ at 0.75 V. These values increase to 0.14 and 1.34 $A g^{-1}$ at the respective potentials after the acid wash. The Tafel slopes are about 37 and 43 mV per decade for acid-wash and non-washed samples, respectively. Although the mass activities are lower than that of Pt/C, they are among the best of cobalt-based ORR catalysts.

An important issue for the ORR catalysis for fuel cell is the number of transferred electrons n, with four being preferred because the mechanism leads to formation of H_2O as the product. We investigated the electron transfer mechanism by using both the RRDE and the Koutecky–Levich methods. A value of n ranging from 3.2 to 3.5 was observed for **1** activated at 750 °C. It was further improved to $3.3 \approx 3.6$ after sonicating in sulfuric acid before preparing the catalyst ink. The results suggest a dominative four electron transfer process with certain peroxide formation. Acid wash removes a significant fraction of unreactive metal particles and improves the catalyst ink dispersion over the electrode surface (see the Supporting Information).

Chemical stability in the acidic environment represents another key issue for TM-based ORR catalysts. The active sites can be "bleached" by the acid, particularly under polarization, leading to loss of catalytic activity. We conducted a chronoamperometry experiment for **1** activated at 750 °C by using the RDE setup. The experiment was carried out in the oxygen-saturated electrolyte of 0.1 M $HClO_4$ aqueous solution. The electrode potential was switched between 0.35 and 0.7 V (RHE) repeatedly with 15 min period dwell time at each potential. We observed that the electrocatalytic activity was stabilized after one and half hour on-stream (see the Supporting Information).

A question one must address when introducing a new catalyst precursor is how its structure affects the catalytic property and active-site formation? We conducted a series of characterizations in an attempt to understand the surface property, morphology, and electronic configuration of key active-site elements during the transformation from **1** to catalyst. The surface property of **1** was well characterized with BET SSA of 305 $m^2 g^{-1}$ and exclusive micropore distribution, as one would expected from its well-defined lattice structure (Table 1). Upon thermal activation, the powder X-ray diffraction shows that the sample underwent a structural transformation and no longer maintains long-range lattice order. The N_2 adsorption isotherm, however, shows that the sample with the best ORR activity retained a BET SSA of 264 $m^2 g^{-1}$ and a significant fraction of the micropore volume after heat-treated at 750 °C. Furthermore, mesopores with dimension ranging from 20 to 40 Å were formed. Increasing the activation temperature to 900 °C led to reduction in SSA from both micropore and mesopore regions, exemplifying the direct correlation between the surface area and the catalyst activity. The Co metal crystallites formed during thermal activation can be dissolved in sulfuric acid through sonication. Such treatment enhanced BET SSA by nearly 70 %, as is given in Table 1. The increase of surface area, however, is mainly contributed by the mesopores. It is important to note that the active catalyst retains a considerable pore volume from the micropores (< 20 Å) which is recognized as a key attribute for non-PGM catalysts[7,13] (see the Supporting Information).

Table 1. Surface properties measured by nitrogen adsorption isotherm at 77 K for **1** after different treatments.

Sample	BET surface area [$m^2 g^{-1}$]	Micropore diameter [Å]	Mesopore diameter [Å]
fresh **1**	305	8–13	N/A[a]
1 activated at 750 °C	264	10–12	20–40
1 activated at 900 °C	142	10–12	20–40
1 activated at 750 °C and acid wash	434	10–12	18–50

[a] N/A = not applicable.

Accompanying the change of surface properties, we also observed transformation of framework morphology through transmission electron microscopy (TEM). For example, the TEM image reveals light-gray spots uniformly distributed over a fine texture background for the sample heated at 500 °C, suggesting a mild agglomeration of a small amount of cobalt segregated from the framework. Increasing temperature to 750 °C darkens the spots indicating further agglomeration of Co. The framework structure images change from smooth to grainier texture, presumably due to crystallinity breakdown and the mesopore formation during the conversion of organic moiety to carbons. A high resolution image shows uneven texture for Co crystallites surrounded by graphene layers. Both metal particles and organic background become more segregated for the sample treated at 900 °C (see the Supporting Information).

X-ray absorption spectroscopy (XAS) is an element-selective tool that can be used to characterize the changes in the cobalt oxidation state and the coordination structure during thermal activation.[17] We investigated **1** treated under different conditions by using X-ray absorption near-edge structure (XANES) and extended X-ray absorption fine structure (EXAFS) spectroscopic techniques at the Co K-edge at the Advanced Photon Source, Argonne National Laboratory. We found that, for the sample activated at 500 °C, both XANES and EXAFS were nearly identical to that of fresh **1**, suggesting that the majority of Co remains in the framework in +2 oxidation state, ligated by the four nitrogens from the imidazolate groups. At higher activation temperatures, however, both XANES and EXAFS showed the formation of finely dispersed cobalt crystallites, of which the size increases with temperature. Sonicating the activate **1** in sulfuric acid reduced the metallic features, indicating substantially removing but not eliminating Co^0 particles. The most intriguing observation is the reappearance of the spectroscopic characteristics associated with Co–N_x both in the near-edge spectrum and the radial-distribution function, which was overshadowed by the metallic cobalt prior to acid washing. More extensive data collection and analysis is re-

quired to accurately account for a Co–N_x structure, which will be reported in the future (see the Supporting Information).

Transformation of C and N in the imidazolate ligand during thermal activation could provide complementary structural evidence regarding to the active-site formation. X-ray photoelectron spectroscopy (XPS) was performed to study the electronic transitions of C and N in **1** before and after heat-treatment. We found that C remained mainly as the original organic moiety at 500 °C, and was converted to carbonaceous (750 °C) and graphitic (900 °C) forms with increase of activation temperature. Meanwhile, N also maintained in the imidazolate form at 500 °C. After activation at 750 °C, XPS showed that N was converted to a mixture of pyridinic- and pyrrolic-like moieties with the former being the dominant component. Further increase of temperature to 900 °C led to a reduction of the N content and even distribution between the pyridinic and pyrrolic forms (see the Supporting Information).

The correlation between the structural evolution and catalytic performance leads us to propose the following mechanism of the active-site formation from the precursor **1**: in the fresh **1**, each Co^{2+} is coordinated by four nitrogen atoms from the neighboring imidazolate groups, as is shown in Figure 1a and Scheme 1a. Upon thermal activation, the imidazolate groups gradually convert to carbonaceous forms whereas a fraction of the nitrogen is retained as pyridinic- or pyrrolic-like moieties. Such moieties are known to form catalytic sites through coordinating the transition metal by nitrogen,[7,10,13] an example is Co–N_4, shown by a proposed structure in Scheme 1b. Loss of hydrogen and some carbon and nitrogen at 750 °C during the conversion from organic ligand to N-containing graphene alters the structure of the framework with the formation of mesopores while maintaining certain fraction of the micropores. Because higher stoichiometric ratios of C and N are needed to form the active site shown in Scheme 1b, than that available in the structure shown in Scheme 1a, excess Co^{2+} ions are segregated from the framework and agglomerated to Co^0. Meanwhile, a fraction of Co^{2+} is stabilized through coordinating with the pyridinic or pyrrolic nitrogen atoms to form Co–N_x. Further increase of temperature to 900 °C graphitizes carbon, causing further loss of N for active sites and therefore, less activity. The segregated Co^0 crystallites contribute little to the ORR activity. In fact, a higher mass activity and SSA have been achieved after a fraction of metallic Co is removed by acid wash. The presence of high concentration of metal as the building unit for MOF represents a key challenge for this approach because our study identified the difficulty of eliminating Co particles encapsulated by carbon. Such metal particles, though highly stable, will add unnecessary weight and unfavorably affect the apparent mass activity in comparison with other low-metal-loading non-PGM catalyst. On the other hand, high level of individually coordinated metal in MOF also presents a unique opportunity of constructing catalyst with the highest active-site density. One potential approach could be better utilization of metal hence, higher active site through increasing ligand C and N ratios to TM in the new MOF design. Although the original MOF structure can not be retained after thermal activation, it plays a crucial role in uniformly distributing Co and N-functional groups in a 3D microporous architecture for producing densely populated active sites while maintaining sufficient porosity and SSA, all are critical for a non-PGM electrocatalysts. This is also distinctly different from making a catalyst by simply mixing chemicals. We proved this point by activating a simple mixture of 3,5-imidazolate and Co-$(NO_3)_2 \cdot 6H_2O$ in the same stoichiometric amount used for preparing **1**. No comparable ORR performance could be reproduced (see the Supporting Information).

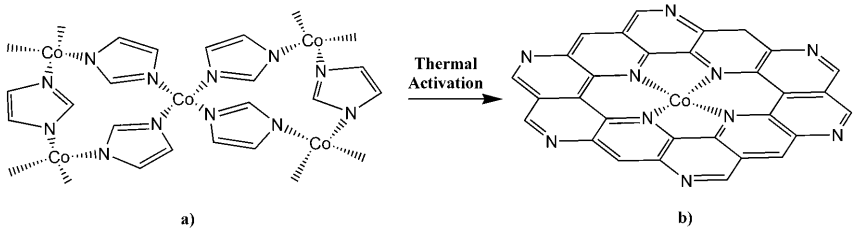

Scheme 1. Proposed structural conversion from **1** to the catalytic active site.

In summary, we have demonstrated for the first time the preparation of a non-PGM electrode catalyst for the oxygen reduction reaction by using cobalt imidazolate framework through thermal activation. Considering the richness of MOF varieties, the work presented here not only introduces a new class of materials with the highest possible precursor-site density and compatible surface property, but also provides a distinct platform with abundant model compounds for studying the correlation between the ligand structure and the catalyst performance. The coordination chemistry and conversion mechanism from different TM–N_4 precursors with well-defined 3D ligation could provide critical insights for further improving non-PGM electrocatalyst performance.

Experimental Section

Synthesis of compound 1: Compound **1** was synthesized according to a procedure similar to previously reported strategies.[15] Briefly, Co-$(NO_3)_2 \cdot 4H_2O$ (3.115 g, >98%), imidazole (1.7 g, >99%), and piperazine (1.075 g, >99%) were added to dimethylacetamide (DMA) (65 mL, >99%). All chemicals were procured from Sigma–Aldrich. The reaction mixture was stirred at room temperature for 2 h until the solution become clear. The solution was then placed in a Teflon-lined autoclave (Parr 4748). The autoclave was sealed and heated in a programmable

oven (Thermo CV800F) to 135 °C with a ramping rate of 1 °C min^{-1}, and maintained at 135 °C for 24 h. After cooling to room temperature at a rate of 0.1 °C min^{-1}, violet prism crystals were collected and washed with DMA (3×10 mL) to give compound **1** (80% based on imidazolate ligand).

Heat and acid treatments: Compound **1** (15 mg) was weighed in a ceramic boat and placed in a quartz tube (diameter = 1″). The tube was sealed airtight and placed inside a furnace, where the material was heat treated at temperatures ranging between 500 and 900 °C. The heat treatment typically runs for 1 h, in flowing Ar at a rate of 100 mL min^{-1}. The yield after the thermal treatment was typically within 40–60%. Acid washing was carried out by sonicating activated **1** in H_2SO_4 (0.5 M or 2 M) for 2 h, followed by continuous agitation at 80 °C for 20 h. The weight loss from the acid wash typically ranges from 30 to 40%. Elemental analysis of a typical sample **1** activated at 750 °C showed molar fractions of 33% of Co, 1.8% of N, and 65% of C. After acid wash, these values were changed to 17% for Co, 2.2% for N, and 81% for C.

Experimental details of RDE, RRDE, BET, TEM, XAS, and XPS studies are given in the Supporting Information.

Acknowledgements

This work and the use of Advanced Photon Source are supported by Office of Science, U.S. Department of Energy under Contract DE-AC02-06CH11357. S.M. acknowledges the Director's Postdoctoral Fellowship from Argonne National Laboratory. Authors wish to thank Professor Louise Liu of Texas A&M for the support of TEM and XPS studies and Dr. Jianglan Shui and Dr. Shengwen Yuan for additional experimental support.

Keywords: cobalt · electrocatalysts · metal–organic frameworks · oxygen reduction reaction

[1] a) S. Masaoka, D. Tanaka, Y. Nakanishi, S. Kitagawa, *Angew. Chem.* **2004**, *116*, 2584–2588; *Angew. Chem. Int. Ed.* **2004**, *43*, 2530–2534; S. Kitagawa, R. Kitaura, S.-I. Noro, *Angew. Chem.* **2004**, *116*, 2388–2430; *Angew. Chem. Int. Ed.* **2004**, *43*, 2334–2375; b) G. Férey, *Chem. Soc. Rev.* **2008**, *37*, 191–214; c) J. R. Long, O. M. Yaghi, *Chem. Soc. Rev.* **2009**, *38*, 1213–1214.

[2] a) M. P. Suh, Y. E. Cheon, E. Y. Lee, *Coord. Chem. Rev.* **2008**, *252*, 1007–1026; b) R. J. Kuppler, D. J. Timmons, Q.-R. Fang, J.-R. Li, T. A. Makal, M. D. Young, D. Yuan, D. Zhao, W. Zhuang, H. Zhou, *Coord. Chem. Rev.* **2009**, *253*, 3042–3066.

[3] a) M. Eddaoudi, J. Kim, N. Rosi, D. Vodak, J. Wachter, M. O'Keeffe, O. M. Yaghi, *Science* **2002**, *295*, 469–472; b) O. M. Yaghi, M. O'Keeffe, N. W. Ockwig, H. K. Chae, M. Eddaoudi, J. Kim, *Nature* **2003**, *423*, 705–714; M. O'Keeffe, *Chem. Soc. Rev.* **2009**, *38*, 1215–1217.

[4] a) D. J. Tranchemontagne, J. L. Mendoza-Cortes, M. O'Keeffe, O. M. Yaghi, *Chem. Soc. Rev.* **2009**, *38*, 1257–1283; b) J. J. Perry IV, J. A. Perman, M. J. Zaworotko, *Chem. Soc. Rev.* **2009**, *38*, 1400–1417.

[5] a) D. J. Collins, H.-C. Zhou, *J. Mater. Chem.* **2007**, *17*, 3154–3160; b) L. J. Murray, M. Dinca, J. R. Long, *Chem. Soc. Rev.* **2009**, *38*, 1294–1314; c) J.-R. Li, R. J. Kuppler, H.-C. Zhou, *Chem. Soc. Rev.* **2009**, *38*, 1477–1504; d) S. Ma, H.-C. Zhou, *Chem. Commun.* **2010**, *46*, 44–53; e) S. Ma, *Pure Appl. Chem.* **2009**, *81*, 2235–2251.

[6] J. Lee, O. K. Farha, J. Roberts, K. A. Scheidt, S. T. Nguyen, J. T. Hupp, *Chem. Soc. Rev.* **2009**, *38*, 1450–1459.

[7] F. Jaouen, J. Herranz, M. Lefèvre, J.-P. Dodelet, U. I. Kramm, I. Herrmann, P. Bogdanoff, J. Maruyama, T. Nagaoka, A. Garsuch, J. R. Dahn, T. Olson, S. Pylypenko, P. Atanassov, E. A. Ustinov, *ACS Appl. Mater. Interfaces* **2009**, *1*, 1623–1639.

[8] *Handbook of Fuel Cells—Fundamentals, Technology & Applications, Vol. 5: Advances in Electocatalysis, Materials, Diagnostics & Durability* (Eds.: W. Vielstich, H. A. Gasteiger, H. Yokokawa), Wiley, New York **2009**.

[9] R. Jasinski, *Nature* **1964**, *201*, 1212–1213.

[10] J. P. Dodelet in *N4-Macrocyclic Metal Complexes* (Eds.: J. H. Zagal, F. Bedioui, J. P. Dodelet), Springer, New York, **2006**, pp. 83–147.

[11] R. Bashyam, P. Zelenay, *Nature* **2006**, *443*, 63–66.

[12] G. Wu, Z. Chen, K. Artyushkova, F. H. Garzon, P. Zelenay, *ECS Trans.* **2008**, *16*, 159–170.

[13] M. Lefèvre, E. Proietti, F. Jaouen, J.-P. Dodelet, *Science* **2009**, *324*, 71–74.

[14] H. A. Gasteiger, S. S. Kocha, B. Sompalli, F. T. Wagner, *Appl. Catal. B* **2005**, *56*, 9–35.

[15] Y.-Q. Tian, Z.-X. Chen, L.-H. Weng, H.-B. Guo, S. Gao, D. Y. Zhao, *Inorg. Chem.* **2004**, *43*, 4631–4635.

[16] A. Bard, L. R. Faulkner, *Electrochemical Methods: Fundamentals and Applications*, Wiley, New York, **1980**.

[17] J. Yang, D.-J. Liu, N. Kariuki, L. X. Chen, *Chem. Commun.* **2008**, 329–331.

Received: October 25, 2010
Published online: January 7, 2011

